State-to-State Reaction Dynamics of CH_3I Photodissociation at 304 nm

Guosheng Li,*,† Yun Kyung Shin, and Hyun Jin Hwang‡

Department of Chemistry, Kyunghee University, Seoul, Korea

Received: August 8, 2005; In Final Form: August 18, 2005

The detailed reaction dynamics of CH_3I photodissociation at 304 nm were studied by using high-resolution long time-delayed core-sampling photofragment translation spectroscopy. The vibrational state distributions of the photofragment, i.e., CH_3, are directly resolved due to the high kinetic resolution of this experiment for the first time. CH_3 radicals produced from $I^*(^3Q_{0+})$, $I(^1Q_1 \leftarrow {}^3Q_{0+})$, and $I(^3Q_1)$ channels are populated in different vibrational state distributions. The $I^*(^3Q_{0+})$ and $I(^3Q_1)$ channels show only progressions in the ν_2'-(a_2'') umbrella bending mode, and the $I(^1Q_1 \leftarrow {}^3Q_{0+})$ channel shows both progression in the ν_2' umbrella bending mode and a small amount of excitation in the ν_1' (a_1') C−H stretching mode. The photodissociation processes from the vibrational hot band of CH_3I ($v_3 = 1$, $v_3 = 2$) were also detected, primarily because of the absorption probability from the vibrational excited states, i.e., hot bands are relatively enhanced. Photofragments from the hot bands of CH_3I show a cold vibrational distribution compared to that from the vibrational ground state of CH_3I. The I* quantum yield and the curve crossing possibility were also studied for the ground vibrational state of CH_3I. The potential energy at the curve crossing point was calculated to be 32 790 cm^{-1} by using the one-dimensional Landau−Zener model.

I. Introduction

The photodissociation of polyatomic molecules has been a very active research field in the past few decades. Methyl iodide has long been the prototype molecule for studying the photodissociation dynamics of polyatomic molecules. It has the advantage of being a quasi-linear system but with more complex vibrational motions than a simple linear triatomic molecule can offer. Its dynamics are also governed by an important curve crossing in the exit channels. This mixture of complexity and simplicity has made the *A* band (210−350 nm) of CH_3I photodissociation reaction the subject of extensive experimental[1−18] and theoretical[19−30] studies.

For the ground state of CH_3I, the last filled orbital is an *e* orbital, and therefore the first excited Rydberg state arises from excitation of an iodine nonbonding *p* electron to the lowest available antibonding molecular orbital, that is the σ^* orbital of the C−I bond.[31] The resulting configuration of the first excited state is $....(a_1)^2(e)^3(a_1^*)^1$, and because of the presence of the iodine atom, spin−orbit coupling is large; therefore, the (Ω_c,ω) coupling can be used for the first excited-state electronic configuration of CH_3I.[32] As the result of the electronic configuration shown above, there are five electronic states in the *A* band of CH_3I: two forbidden states, $^3Q_2(1E)$ and $^3Q_{0-}(1A_2)$, one strong parallel repulsive state, $^3Q_{0+}(2A_1)$, and two weak perpendicular repulsive states, $^1Q_1(3E)$ and $^3Q_1(2E)$.[33,34] While the $^1Q_1$ and $^3Q_1$ states correlate to the ground-state $I(^2P_{3/2})$ fragment (labeled as I), the $^3Q_{0+}$ state correlates to the spin−orbit excited-state $I^*(^2P_{1/2})$ fragment (labeled as I*), and it is also known that the $^3Q_{0+}$ potential surface undergoes a branching at the curve crossing point with the $^1Q_1$ surface to give both I and I* fragments as shown as eqs 1a−d.[1]

$$CH_3I \rightarrow CH_3 + I(^1Q_1, \beta = -1) \quad (1a)$$

$$\rightarrow CH_3 + I^*(^3Q_{0+}, \beta = 2) \quad (1b)$$

$$\rightarrow CH_3 + I(^1Q_1 \leftarrow {}^3Q_{0+}, \beta = 2) \quad (1c)$$

$$\rightarrow CH_3 + I(^3Q_1, \beta = -1) \quad (1d)$$

Gedanken et al.[35] determined the parallel transition to $^3Q_{0+}$ has its absorption maximum at 261 nm, and the perpendicular transition to $^1Q_1$ and $^3Q_1$ have their absorption maximum at 240 and 300 nm, respectively. They also determined that the percentage ratio of the total absorption strengths are 78%:21%:1% for $^3Q_{0+}$, $^1Q_1$, and $^3Q_1$ transitions, respectively, by using the magnetic circular dichroism method.

Riley and Wilson[1] did the first work on CH_3I photodissociation at 266 nm nearly 30 years ago, by using the photofragment translation spectroscopy. Early workers[2−5] suggested that the CH_3 radical produced from CH_3I at the *A* band would be left in an inverted vibrational distribution of the ν_2' (a_2'') umbrella-bending mode. Loo et al.[8] used multiphoton ionization to determine that the CH_3 radical, which was produced from the I* channel in 266 nm photodissociation of CH_3I, was left mainly in the vibrational ground state. A number of additional experiments[11,16,17] and theoretical calculations[25−29] showed that the vibrational distribution of CH_3 from the I* channel in the CH_3I *A* band has the strongest distribution in the vibrational ground state, which is a disagreement with the inverted distribution suggested by the earlier workers. The ν_2' (a_2'') umbrella-bending mode is not the only mode excited in the CH_3 radical; the ν_1' (a_1') C−H stretching mode of CH_3 radical was also found to be excited in other expriments.[16,17] Recently, we presented a well resolved vibrational distribution of the CH_3 radical for the I* and I channels for the 266 nm photolysis of CH_3I.[18] At a lower photon energy, the excitation to the $^3Q_1$ state cannot be ignored, because its absorption maximum is near 300

* To whom correspondence should be addressed. E-mail: guoshenl@usc.edu.

† Present address: Department of Chemistry, University of Southern California, L.A., CA 90089.

‡ Present address: Ahram Biosystems, Inc., Seoul 133-833, South Korea.

10.1021/jp054421k CCC: $30.25
Published on Web 09/28/2005

nm.[35] It was reported that the relative absorption strength of the $^3Q_1$ state is ~25% at 304 nm. It was also found that the I* quantum yield at 304 nm photodissociation was significantly lower than that at 266 nm.[13,15]

One of the most important questions still not fully answered is the distribution of the vibrational energy in the dissociation fragments arising from different initial states, from direct photodissociation, and via curve crossing pathways. The main motivation of this work is to use a high-resolution, long time-delayed, pulsed core-sampling photofragment translation spectroscopy to directly resolve the vibrational state distributions of CH_3 radicals produced in 304 nm photodissociation, which has not been shown precisely. By combining with the previously published results of 266 nm photodissociation, we try to give a clear picture of the reaction dynamics for photodissociation in the *A* band of CH_3I.

II. Experimental Section

The experimental setup has been described elsewhere[18] and consists of a single stage pulsed acceleration time-of-flight (TOF) mass spectrometer and a pulsed supersonic molecular beam system. A pulsed nozzle (General valve, Nozzle orifice 0.5 mm) was operated with a pulse width of 250 μs at 10 Hz repetition rate. Ar (99.9999%) was used as a carrier gas, and the expansion pressure was varied between 1 and 2 atm. A pulsed supersonic molecular beam with 4% CH_3I (99.5%, Aldrich) seeded in the carrier gas was collimated by two skimmers and crossed with the laser beam (~304 nm dye beam) in the TOF mass spectrometer.

The laser pulse near 304 nm was generated by frequency doubling the output of a pulsed dye laser (QUANTEL, TDL-90) pumped by the second harmonic beam of the Nd:YAG laser (QUANTEL, YG980). The polarized laser was focused on the molecular beam by a best-form UV quartz lens (focal length is 25 cm), after passing through a half wave plate and a glan polarizer. In this work, to state-selectively ionize via 2+1 REMPI, the laser was set to 304.02 nm for the spin−orbit excited I* and 304.67 nm for ground-state I.

After photodissociation and REMPI, the produced ions spread out in the space and make the ion packages in a few microseconds (8 μs), before the acceleration electric field is applied. The distributions of these ion packages are just a direct reflection of their recoil velocity distributions and directions. While a high voltage pulse (1450 V, 3 μs) is applied to the extraction electrode to accelerate the ion packages to the detector, the ions acquire different acceleration potentials according to their one-dimensional positions along the direction of the acceleration electric field. Finally, the accelerated ions were projected onto a chevron microchannel plate detector (MCP, Galileo Electrooptic). A stainless steel plate (discrimination electrode) with a 3.0 mm diameter hole at the center is mounted at the front of the MCP detector to improve the kinetic energy resolution of photofragment ions. The MCP detector and the discrimination electrode are set 15 mm off to the centerline of the acceleration electrodes in order to compensate for the molecular beam velocity. At a typical experimental condition, the front of the MCP detector is held at a negative high voltage (−1700 V). The signal from the MCP was recorded by an oscilloscope (LeCroy, 9350A, 500 MHz) through Preamplifier (SRS445) and stored in a Pentium 150 MHz computer.

III. Results

The details of the TOF equations and the spectrum analysis method for this long time-delay core-sampling PTS were given elsewhere[18] and will not be repeated here.

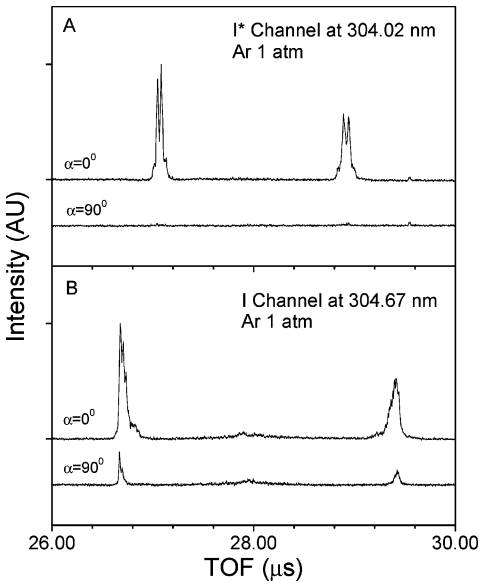

Figure 1. (A) TOF spectrum of resonantly ionized I* photofragment following 304.02 nm photolysis. (B) TOF spectrum of resonantly ionized I photofragment following 304.67 nm photolysis. The delay time between the laser pulse and the high voltage electric pulse is set at 8.0 μs, and the expansion pressure of the pulsed molecular beam is 1 atm for both spectra. The upper and lower spectra correspond to the photolysis laser polarization angle, $\alpha = 0°$ and 90° with respect to the *z*-axis; both spectra averaged 100 000 laser shots.

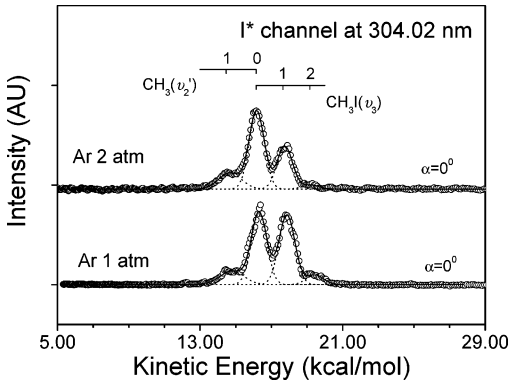

Figure 2. An expanded view of the I* photofragment kinetic energy spectrum, with expansion pressures for the pulsed molecular beam of 1 and 2 atm, respectively. The dotted curves are best fits for the observed vibrational bands, and the solid line is the sum of those fits.

Two main peaks including several vibrational features are observed in each TOF spectrum of I* and I photofragments, which were produced by the photodissociation of CH_3I at 304.02 and 304.67 nm, respectively, as shown in Figure 1. The earlier and later TOF peaks correspond to the same recoil velocity distribution, with the directions away from and toward the MCP detector, respectively. By careful studies, it was found that the energy spacing of three peaks from the right were consistent with a vibrational quantum of 528 cm^{-1}, corresponding to the ν_3 mode[36] (C−I stretching mode of CH_3I), and the energy spacing between the first and the second peaks from the left was consistent with 606 cm^{-1}, corresponding to the ν_2' mode[37] (umbrella bending mode of CH_3 radical). The peaks from the hot bands were significantly reduced in intensity when the expansion pressure of the carrier gas was increased from 1 to 2 atm, as shown as Figure 2. The third peak from the right side in Figure 2 was reasonably assigned as the $CH_3(\upsilon_2' = 0)$ state that photodissociated from the ground state of $CH_3I(\upsilon = 0)$. By following the energy conservation rule, the calculated value

TABLE 1: Vibrational Populations, Rotational Temperatures, and Anisotropy Parameters of CH_3 Photofragment Produced in the I* Channel at 304.02 nm with Backing Pressure Changed

	parent state (CH_3I)				
	$v = 0$			$v_3 = 1$	$v_3 = 2$
fragment state (CH_3)	$v_2' = 0$	$v_2' = 1$	$v_2' = 2$	$v_2' = 0$	$v_2' = 0$
$P(v)$, ($^3Q_{0+}$)	0.85	0.15	<0.01	0.47	0.05
Ar 2 atm					
$P(v)$, ($^3Q_{0+}$)	0.86	0.14	<0.01	0.91	0.16
Ar 1 atm					
β	1.94 ± 0.04	1.88 ± 0.16	...	1.92 ± 0.07	1.80 ± 0.19
E_{vib}, cm^{-1}	0	606	1288	528	1056

of the bond dissociation energy is in excellent agreement with the value 55.80 ± 0.5 kcal/mol of 266 nm photodissociation.[18]

A. Vibrational Distributions of CH_3 Radical at ~304 nm. The vibrationally resolved kinetic energy distribution of the I* photofragment produced at 304.02 nm is shown in Figure 2. Because the I* photofragments are produced from CH_3I in different initial vibrational states, it is necessary to distinguish the distribution from the vibrational ground state of the parent molecule from the contributions of the hot bands. In this experiment, Ar gas was used as a carrier gas in the pulsed molecular beam, and the backing pressure was varied in order to achieve different vibrational cooling conditions for the parent molecule CH_3I. As shown in Figure 2, the hot band distributions dramatically increased as the molecular beam expansion pressure decreased. It was also found that there are no significant changes for the CH_3 radical vibrational distribution originally from the vibrational ground-state CH_3I ($v = 0$), while the hot band distributions are increasing in the intensity, as shown as in Table 1. It is reasonable to suppose that CH_3 radicals produced by photodissociation from the vibrationally hot CH_3I molecules are mostly in their ground state, and the contamination from the CH_3I ($v_3 = 1$) and CH_3I ($v_3 = 2$) photodissociation to CH_3I ($v = 0$) photodissociation is sufficiently small to be ignored. The distribution of CH_3 ($v_2' = 0$) and CH_3 ($v_2' = 1$) from CH_3I ($v = 0$) is determined to be 0.85:0.15 as shown in Table 1. The anisotropy parameters for the ground state and the hot bands are both close to the maximum parallel anisotropy parameter ($\beta = 2$) within error bounds. Since the ν_3 mode is symmetric along the C−I dissociation coordinate, the vibrational excitation in the ν_3 mode of CH_3I will have no change on anisotropy parameters of photofragments.

The kinetic energy distributions of the I photofragment are shown in Figure 3, where the open circles and the open squares correspond to the I photofragment determined with the laser polarization parallel and perpendicular to the detection axis, i.e., $\alpha = 0°$ and $\alpha = 90°$, respectively. From the excited-state potential surfaces of CH_3I, it is known that the I* channel associated with the $^3Q_{0+}$ transition; the I channel determined with $\alpha = 0°$ is produced through the curve crossing process via $^1Q_1 \leftarrow {}^3Q_{0+}$, and the I channel determined with $\alpha = 90°$ is from the direct dissociation from $^3Q_1$ transition. The vibrational energy spacing for the ν_2' umbrella bending mode $v_2' = 0$, 1, 2, and 3 are 0, 606, 1288, and 2019 cm^{-1},[36] and the ν_1' C−H stretching mode $v_1' = 0$ and 1 are 0 and 3004 cm^{-1}, respectively.[38] The assignment of the vibrational state of CH_3 radical produced from $^1Q_1 \leftarrow {}^3Q_{0+}$, i.e., curve crossing process, is shown in Figure 3. The bond energy calculated from the above assignment is also in excellent agreement with the value calculated from the I* channel. It was found that the CH_3 radicals produced from the I channel ($\alpha = 0°$), i.e., through the curve crossing process, are mainly distributed in the ν_2' mode and with a little in the ν_1' mode, as shown in Figure 3 and Table 2. The vibrational distributions for C−H stretching mode are

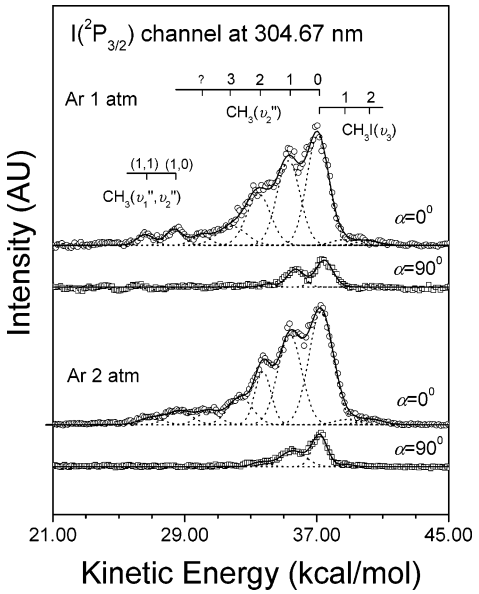

Figure 3. Expanded view of the I photofragment kinetic energy scale with expansion pressures for the pulsed molecular beam of 1 and 2 atm, respectively. The open circles are the experimental spectra with the laser polarization parallel ($\alpha = 0°$) to the detection axis, and the solid line is the summed data of fitting components. The open squares are experimental data with the laser polarization perpendicular ($\alpha = 90°$) to the detection axis.

$v_1' = 0{:}1 = 0.93{:}0.07$. The vibrational distributions are $v_2' = 0{:}1{:}2{:}3 = 0.38{:}0.28{:}0.18{:}0.07$ for $v_1' = 0$, and $v_2' = 0{:}1 = 0.04{:}0.03$ for $v_1' = 1$. There is an unassigned vibrational state in the I channel, as shown in Figure 2 and Table 2. This state is close to the $v_2' = 4$ level of the CH_3 radical; however, the intensity of this state drops down while increasing the expansion pressure. This observation means that there are probably some contributions of CH_3 ($v_3' = 1$) from the hot band of CH_3I ($v_3 = 1$).

The spectrum of the I photofragments determined with $\alpha = 90°$ is associated with the $^3Q_1$ transition of CH_3I and is shown in Figure 3. There are no hot bands of CH_3I observed in the $^3Q_1$ transition, which is quite reasonable because the $^3Q_1$ transition is a low-lying transition compared with $^3Q_{0+}$ and the absorption strength of $^3Q_1$ state is not enhanced for the ν_3 mode excited CH_3I molecule. The CH_3 radicals, produced from excitation to the $^3Q_1$ state of the CH_3I, show only a progression in the ν_2' umbrella-bending mode. The distributions of the ν_2' mode are $v_2' = 0{:}1{:}2 = 0.58{:}0.35{:}0.07$.

B. I* Quantum Yield and Curve Crossing Possibility. A calibration method that can determine the I* quantum yield by using the core-sampling PTS method has been reported elsewhere.[15] State-selective ionization of iodine atoms from one-photon photodissociation are followed by 2+1 REMPI within the same laser power for the I* and the I channels. Signal ratio

TABLE 2: Vibrational Populations and the Anisotropy Parameters of CH_3 Photofragment Produced in the I Channel at 304.67 nm with the Different Expansion Pressures of the Carrier Gas

	parent state (CH_3I)								
	$v = 0$							$v_3 = 1$	$v_3 = 2$
fragment (CH_3)	$v_2' = 0$	$v_2' = 1$	$v_2' = 2$	$v_2' = 3$	?	$v_1' = 1, v_2' = 0$	$v_1' = 1, v_2' = 1$	$v_2' = 0$	$v_2' = 0$
$P(v)$ ($^3Q_{0+} \rightarrow {}^1Q_1$) Ar 2 atm	0.38	0.28	0.18	0.07	0.02	0.04	0.03	0.02	0.01
$P(v)$, ($^3Q_1$) Ar 2 atm	0.58	0.35	0.07	<0.01	...	...	...	...	...
$P(v)$ ($^3Q_{0+} \rightarrow {}^1Q_1$) Ar 1 atm	0.37	0.29	0.16	0.08	0.04	0.04	0.02	0.02	0.01
$P(v)$, ($^3Q_1$) Ar 1 atm	0.60	0.32	0.08	<0.01	...	...	...	...	...
E_{vib}, cm^{-1}	0	606	1288	2019	2496 or 2790	3004	3610	528	1056

TABLE 3: I* Quantum Yield (Φ*), the Curve Crossing Possibility (P_{cc}), and the Absorption Strength (σ) at 304 nm

excited state (CH_3I)	product channel	Φ* ($v = 0$)	P_{cc} (%)	σ (%)
$^3Q_0$	I*	0.07 ± 0.02	...	$76\% \pm 4$
	I	0.69 ± 0.02	$92\% \pm 4$	
$^3Q_1$	I	0.24 ± 0.02	...	$24\% \pm 4$

for each channel in eq 1 can be shown as

$$\frac{S^*(^3Q_{0+})}{S(^3Q_{0+} \rightarrow {}^1Q_1)} = \frac{\sigma^*}{\sigma} \cdot \frac{F(^3Q_{0+})}{F(^3Q_{0+} \rightarrow {}^1Q_1)} \cdot \frac{\sigma_R(I^*)}{\sigma_R(I)} \cdot \frac{N(^3Q_{0+})}{N(^3Q_{0+} \rightarrow {}^1Q_1)} \quad (2)$$

$$\frac{S^*(^3Q_{0+})}{S(^3Q_1)} = \frac{\sigma^*}{\sigma} \cdot \frac{F(^3Q_{0+})}{F(^3Q_1)} \cdot \frac{\sigma_R(I^*)}{\sigma_R(I)} \cdot \frac{N(^3Q_{0+})}{N(^3Q_1)} \quad (3)$$

where σ^* and σ represent the absorption cross-sections of CH_3I at 304.02 and 304.67 nm, respectively. Because 304.02 and 304.67 nm are very close within the *A* band of CH_3I, the σ^* and σ can be assumed equal. *F* is the detection efficiency of the iodine atom through the discrimination hole electrode, which can be calculated exactly.[39] The $\sigma_R(I^*)$ and $\sigma_R(I)$ are the 2+1 photon REMPI line strengths for I* at 304.02 nm and I at 304.67 nm, respectively. The line strength ratio of I*:I is determined as 0.78 ± 0.06 in this experiment, by using an I_2 photolysis at 304 nm which yields equal amounts of I and I*.[40] Our value 0.78 ± 0.06 is consistent with 0.80 ± 0.05[15] and 0.77 ± 0.11[41] published before, from a method similar to this experiment. *N* is the real number of iodine atoms produced from 304 nm photodissociation of CH_3I. By determining the signal intensity ratio at the same laser pulse energy, it is possible to calculate the real iodine atom ratio produced from three different channels. The I* quantum yield, the curve crossing possibility, and the relative absorption strengths of each excited state are shown in Table 3.

The simplest approach to the curve crossing in one dimension is the Landau−Zener theory[40] that enables one to calculate the curve crossing probability. A modified one-dimensional Landau−Zener probability is shown as below[15,42]

$$\phi^* = \exp\left(-\frac{\zeta_m}{2(E_{hv} - E_c)^{1/2}}\right) \quad (4)$$

where ζ_m is the modified Landau−Zener parameter, E_{hv} is the photodissociation energy, and E_c is the potential energy of the photofragment at the crossing point. By measuring the I* quantum yield at two different wavelengths, E_c can be obtained from

$$\frac{E_{hv_1} - E_c}{E_{hv_2} - E_c} = \left(\frac{\ln \phi_2^*}{\ln \phi_1^*}\right)^2 = K \quad (5a)$$

$$E_c = \frac{K \cdot E_{hv_2} - E_{hv_1}}{K - 1} \quad (5b)$$

The I* quantum yield in the 304 nm photodissociation measured in this experiment was 8%, and the I* quantum yield was determined as 69% in 266 nm photodissociation of CH_3I.[39] Substituting these values into eqs 5a and 5b, the potential energy at curve crossing point is calculated to be 32 790 cm^{-1}.

IV. Discussion

Theoretical studies of the *A* band photodissociation of CH_3I have been performed over the 30 years. Shapiro and Bersohn[19] treated CH_3I photodissociation as a collinear pseudotriatomic model system. In this model, the empirical two-dimensional potential surfaces for the ground state and the excited state were constructed to reproduce the early experimental data at 266 nm.[2] The first ab initio potential energy surface that allows for detailed understanding of the photodissociation reaction dynamics of CH_3I was developed by Amatatsu et al.[24] Hammerich et al.[29] has calculated the CH_3I photodissociation process by multidimensional wave packets with five-dimensional ab initio potential energy surfaces. Recently, Amatatsu et al.[30] also has calculated full nine-dimensional ab initio potential energy surfaces of CH_3I, and they used surface hopping quasiclassical trajectory calculations on these potential surfaces to study photodissociation dynamics of CH_3I in the *A* band.

The directly resolved vibrational distributions of the CH_3 radical for I* and I channels at 266 and 304 nm are shown in Figure 4. Comparing these data at two different wavelengths, it is clear that the CH_3 radical produced via the I* channel ($^3Q_{0+}$) is vibrationally cooler than that produced via the I channel ($^1Q_1 \leftarrow {}^3Q_{0+}$) and that the umbrella bending mode and the C−H stretching mode vibrational distributions in I* ($^3Q_{0+}$) and I ($^1Q_1 \leftarrow {}^3Q_{0+}$) channels are shifted to a lower quantum number, while the photodissociation wavelength increases. The vibrational distributions of the I* and I channels at the *A* band photodissociation have been studied by a number of theoretical methods,[27−29] and the trend of the calculated vibrational distribution is basically consistent with experimental results in this work.

The weak perpendicular transition $^3Q_1$ has not been studied in any detail either experimentally or theoretically, mostly

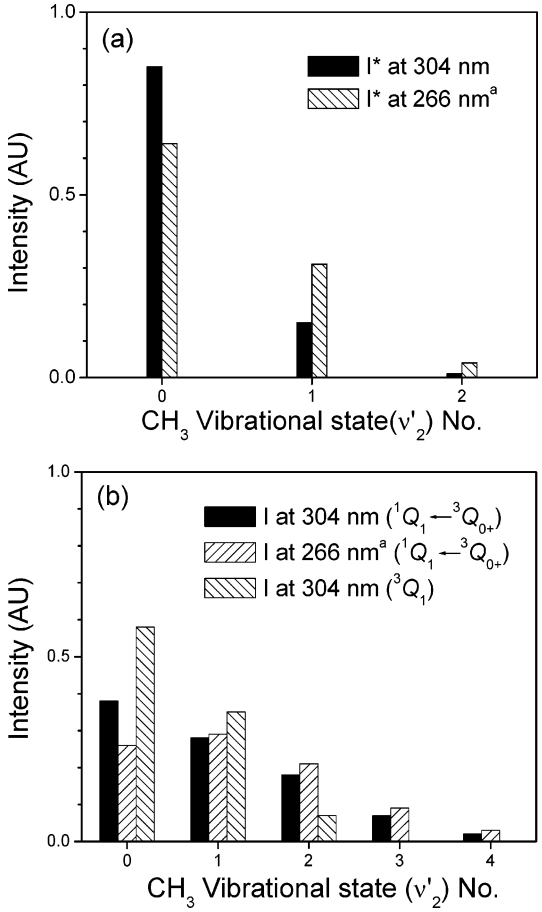

Figure 4. The vibrational state distribution of CH_3 radical at 304 and 266 nm: (a) is for the I* channel and (b) is for the I channel. [a]Reference 18.

because of the low transition probability. As shown in Figure 4, the vibrational distributions for the $^3Q_1$ transition are much cooler than those of $^1Q_1 \leftarrow {}^3Q_{0+}$, via curve crossing process. However, it shows slightly hotter vibrational distributions comparing to those from the $^3Q_{0+}$ state. This might be due to the different potential energy surface of the $^3Q_{0+}$ and $^3Q_1$ states, which comes from the result that the Franck−Condon envelope is kept further away from the reaction coordinate for the $^3Q_1$ state compared to the $^3Q_{0+}$ state.

The observed product from the hot band suggests that it is due to the large enhancement in the absorption cross-section of the $CH_3I(v_3 = 1)$ and $CH_3I(v_3 = 2)$ compared with the ground vibrational state $CH_3I(v = 0)$. This enhancement in the absorption cross-section for initial ν_3 via the C−I stretching mode excited molecule is consistent with the recent experimental results of Eppink et al.[17] The results of vibrational distributions of the hot band CH_3I photolysis in this work show that the CH_3 are produced in lower vibrational states compared to those from the vibrational ground state of CH_3I. This feature of the dynamics feature is also consistent with the trends studied by the theoretical calculations.[24,26]

Determining the contamination of the vibrational hot band is important because the absorption cross-sections of the CH_3I vibrational excited in the ν_3 mode are greatly enhanced compared to the vibrational ground-state CH_3I in the $^3Q_{0+}$ transition.[43] Although, the cooling of the parent molecule CH_3I seeded in a molecular beam will change with a different carrier gas, the pressure of carrier gas, and nozzle pulse width, the portion of the signal arising from the vibrational hot CH_3I photodissociation cannot be neglected. As described above, 32 790 cm^{-1} is obtained by only considering the photodissociation from the vibrational ground state. Kang et al.[15] reported the potential energy at a curve crossing point as 32 200 cm^{-1}, which is lower by 590 cm^{-1} compared to this work. This lower estimation of the potential energy might be due to the contamination of the hot bands of CH_3I for the I* quantum yield in their experiment. Tadjeddine et al.[21] calculated the potential energy at the curve crossing point as 31 100 cm^{-1} by the ab initio method and 30 716 cm^{-1} in Shapiro's model potential.[19] Comparing these data, it can be easily recognized that the potential energies determined by the experimental method are quite similar with each other, but the theoretical data showed a slight difference from the experimental data. These differences probably come from the steep nature of the potential energy surface of the $^1Q_1$ state; the small change in the C−I bond length at a curve crossing point in the theoretical calculation will produce quite a large change in the potential energy of the curve crossing point.[10]

V. Conclusions

Detailed information on the reaction dynamics of the CH_3 radical produced from CH_3I by photodissociation at 304 nm was determined with a high-resolution photofragment translational spectroscopy in this work. This high-resolution allows a detailed confirmation of earlier theoretical calculations of trends to the vibrational state distributions. New features of the $^3Q_1$ state were also observed in this experiment. The I* quantum yield was carefully determined by eliminating contamination from hot bands.

Acknowledgment. This experiment was supported by special instrument maintenance funding from the Korea Science and Engineering Foundation. Authors thank Dr. Dows and Dr. Pratt for correcting the manuscript.

References and Notes

(1) Riley, S. J.; Wilson, K. R. *Faraday Discuss. Chem. Soc.* **1972**, *53*, 132.
(2) Sparks, R. K.; Shobatake, K.; Carlson, L. R.; Lee, Y. T. *J. Chem. Phys.* **1981**, *75*, 3838.
(3) Hermann, H. W.; Leone, S. R. *J. Chem. Phys.* **1982**, *76*, 4766.
(4) Barry, M. D.; Gorry, P. A. *Mol. Phys.* **1984**, *52*, 461.
(5) Van veen, G. N. A.; Baller, T.; Vries, A. E. De.; Van veen, N. J. A. *Chem. Phys.* **1984**, *87*, 405.
(6) Black, J. F.; Powis, I. *Chem. Phys.* **1988**, *125*, 375.
(7) Continetti, R. E.; Balko, B. A.; Lee, Y. T. *J. Chem. Phys.* **1988**, *89*, 3383.
(8) Loo, R. O.; Haerri, H.-P.; Hall, G. E.; Houston, P. L. *J. Chem. Phys.* **1989**, *90*, 4222.
(9) Chandler, D. W.; Chandler; Thoman, J. W., Jr.; Janssen, M. H. M.; Parker D. H. *Chem. Phys. Lett.* **1989**, *156*, 151.
(10) Lao, K. W.; Person, M. D.; Xayariboun P.; Butler, L. J. *J. Chem. Phys.* **1990**, *92*, 823.
(11) Suzuki, T.; Kanamori, H.; Hirota, E. *J. Chem. Phys.* **1991**, *94*, 6607.
(12) Zahedi, M.; Harrison, J. A.; Nibler, J. W. *J. Chem. Phys.* **1993**, *100*, 4043.
(13) Hertz, R. B.; Syage, J. A. *J. Chem. Phys.* **1994**, *100*, 9265.
(14) Johnson, B. R.; Kittrell, C.; Kelly, P. B.; Kinsey, J. L. *J. Phys. Chem.* **1996**, *100*, 7743.
(15) Kang, W. K.; Jung, K. W.; Kim, D.-C., Jung, K.-H. *J. Chem. Phys.* **1996**, *104*, 5815.
(16) Eppink, A. T. J. B.; Parker, D. H. *J. Chem. Phys.* **1998**, *109*, 4758.
(17) Eppink, A. T. J. B.; Parker, D. H. *J. Chem. Phys.* **1999**, *110*, 832.
(18) Li, G.; Hwang, H. J.; Jung, H. C. *Rev. Sci. Instrum.* **2005**, *76*, 023105.
(19) Shapiro, M.; Bersohn, R. *J. Chem. Phys.* **1980**, *73*, 3810.
(20) Shaprio, M. *J. Phys. Chem.* **1986**, *90*, 3653.
(21) Tadjeddine, M.; Flament, J. P.; Teichteil, C. *Chem. Phys.* **1987**, *118*, 45.
(22) Yabushita S.; Morokuma, K. *Chem. Phys. Lett.* **1988**, *153*, 517.
(23) Guo, H.; Schatz, G. C. *J. Chem. Phys.* **1990**, *93*, 393.

(24) Amatatsu, Y.; Morokuma, K.; Yabushita, S. *J. Chem. Phys*. **1991**, *94*, 4858.
(25) Guo, H. *Chem. Phys. Lett*. **1991**, *197*, 360.
(26) Guo, H.; Lao, K.; Schatz, G. C.; Hammerich, A. D. *J. Chem. Phys*. **1991**, *94*, 6562.
(27) Guo, H. *J. Chem. Phys*. **1992**, *96*, 6629.
(28) Rist, C.; Alexander, M. H. *J. Chem. Phys*. **1993**, *98*, 6196.
(29) Hammerich, A. D.; Manthe, U.; Kosloff, R.; Meyer, H.; Cederbaum, L. S. *J. Chem. Phys.* **1994**, *101*, 5623.
(30) Amatatsu, Y.; Yabushita, S.; Morokuma, K. *J. Chem. Phys*. **1996**, *104*, 9783.
(31) Mulliken, R. S.; Teller, E. *Phys. Rev*. **1942**, *61*, 283.
(32) Herzberg, G. *Molecular Spectra and Molecular Structure III. Electronic Spectra and Electronic Structure of Polyatomic Molecules*; van Nostrand: Princeton, 1966.
(33) Mulliken, R. S. *Phys. Rev*. **1936**, *50*, 1017.
(34) Mulliken, R. S. *J. Chem. Phys*. **1940**, *8*, 382.
(35) Gedanken, A.; Rowe, M. D. *Chem. Phys. Lett*. **1975**, *34*, 39.
(36) Hale, M. O.; Galica, G. E.; Glogover, S. G.; Kinsey, J. L. *J. Phys. Chem*. **1986**, *90*, 4997.
(37) Yamada, C.; Hirota, E.; Kawaguchi, K. *J. Chem. Phys*. **1981**, *75*, 525.
(38) Triggs, N. E.; Zahedi, M.; J. Nibler, W.; Debarber, P.; Valentini, J. J. *J. Chem. Phys*. **1992**, *96*, 1822.
(39) Li, G. Ph.D. Dissertation, Kyunghee University, Seoul, South Korea, 2003.
(40) Clear R. D.; Wilson K. R. *J. Mol. Spectrosc*. **1973**, *47*, 39.
(41) Hwang, H. J.; El-Sayed, M. A. *J. Phys. Chem*. **1992**, *95*, 8044.
(42) Godwin, F. G.; Paterson, C.; Gorry, P. A. *Mol. Phys.* **1987**, *61*, 827.
(43) Shinke R. *Photodissociation Dynamics. Spectroscopy and Fragmentation of Small Polyatomic Molecules*; Cambridge University Press: Cambridge, 1993; p 315.